Stochastic Environmental Research and Risk Assessment (2025) 39:4107–4124
https://doi.org/10.1007/s00477-025-03052-7

ORIGINAL PAPER

Seasonal and annual precipitation characteristics of Türkiye and the influence of atmospheric-ocean interactions

Musa Esit[1] · **Mehmet Ishak Yuce**[2] · **Islam Yasa**[3] · **Ibrahim Halil Deger**[4]

Accepted: 27 June 2025 / Published online: 12 July 2025

Abstract
This study explores the relationship between Türkiye's precipitation series and major climate indices, including AMO, PDO, and Nino 3.4. The analysis reveals significant spatial variability in precipitation across Türkiye, with coastal regions like the Black Sea and Mediterranean receiving higher rainfall compared to Central Anatolia. The seasonal distribution shows a distinct north-south gradient, with winter precipitation concentrated in the west and south, while summer precipitation is more intense in the southern and southeastern regions. Precipitation Concentration Index (PCI) and Coefficient of Variation (CV) analyses highlight the diverse hydroclimate across the country. Coastal areas, particularly in the south and west, exhibit high seasonal concentration and variability, while the Black Sea coast experiences more uniform precipitation year-round. Decadal analysis of the PCI reveals shifts in precipitation patterns over the past four decades, with notable changes in the 1980s, 2000s, and 2010s. Cross-Wavelet Transform (XWT) analyses show that the AMO (Atlantic Multidecadal Oscillation) exerts a long-term influence on precipitation, particularly in the Mediterranean and Eastern Anatolia regions, while the PDO (Pacific Decadal Oscillation) significantly impacts Southeastern Anatolia. However, Nino 3.4 exhibits more intermittent effects. Same-year correlations between these indices and precipitation are generally stronger than lagged correlations, indicating more immediate impacts. As a result of XWT, the post-2000 period shows shifts in climate dynamics and teleconnections, suggesting evolving influences on Türkiye's precipitation, and underscoring the need for adaptive water management strategies.

Keywords Precipitation · Trend · Climate indices · XWT · Türkiye

1 Introduction

Precipitation is a substantial natural mechanism that plays a key role in the Earth's water cycle, energy balance, and climate patterns. It influences global and regional climates through its impact on streamflow, groundwater, temperature, humidity, and atmospheric composition (Akdi and Ünlü 2021; Aksu et al. 2022; Yu et al. 2023; Safdar et al. 2023; Lu et al. 2023; Zhang et al. 2024). Over the past several decades, climate change has intensified the movement of water between terrestrial areas and oceans, altering the dynamics of the hydrologic cycle (Voigt and Shaw 2015; Lu et al. 2023). Climate simulations consistently predict that worldwide average precipitation will increase by approximately 1 to 3% for each degree of global temperature rise (Held and Soden 2006; IPCC 2013). The Intergovernmental Panel on Climate Change reported that in the 20th century, global temperatures increased by approximately 0.4 to 0.8 degrees Celsius. Based on six different scenarios, this value may rise by 1.8 to 4 degrees Celsius by the end of the 21st century (Mullick et al. 2019; Ahmadi et al. 2022).

Precipitation and temperature are the primary drivers of the water cycle, and they have a direct impact on the availability of water resources in a given region (Yang et al. 2020; Qamar et al. 2022). Precipitation, being the principal source of water, plays a vital role in supporting and

✉ Musa Esit
mesit@adiyaman.edu.tr

1 Civil Engineering Department, Adiyaman University, Adiyaman, Türkiye

2 Civil Engineering Department, Gaziantep University, Gaziantep, Türkiye

3 Civil Engineering Department, Ondokuz Mayis University, Samsun, Türkiye

4 Civil Engineering Department, Hasan Kalyoncu University, Gaziantep, Türkiye

advancing society, economy, and environment (Guo et al. 2020; Zhang et al. 2022). Precipitation has undergone substantial changes due to climate change (Dore 2005; Huang et al. 2016; Ren et al. 2017; Tabari 2020), such as meteorological drought (Dore 2005; Abbas and Kousar 2021), flood (Guhathakurta et al., 2011; Kundzewicz et al. 2014; Lehner et al. 2006), and changes in precipitation concentration (Dong et al. 2021; Ashrafi et al. 2024). In addition, the higher temperatures cause an increase in atmospheric water vapor, resulting in more intense precipitation events (Liu et al. 2020). However, warmer temperatures also intensify evaporation and transpiration, increasing the risk of longer, more severe droughts (Mishra et al. 2010; Dai et al. 2018). Therefore, understanding changes in precipitation is crucial for studying environmental shifts.

Recent studies have investigated monthly, seasonal, and annual changes in precipitation variability at global and regional scales (Alexander et al. 2006; Fischer and Knutti 2015; Hao et al. 2019; Esit et al. 2021; Kim et al. 2023; Salameh 2024). Examples include studies where Wai et al. (2017) observed long-term precipitation trends linked to urbanization and their implications for sustainable urban development. The study analyzed a 10-year precipitation dataset for a rapidly urbanized megacity and nearby suburban/rural areas in southern China. There was a statistically significant, long-term increasing trend of precipitation (45.6 mm per decade) found only at the megacity station, not at the other stations. Kundzewicz et al. (2014) studied on flood risk in a changing climate: global and regional insights. They assessed changes in flood risk across seven regions, based on the IPCC SREX report and new literature. Sarkar and Maity (2020) demonstrated rising extreme rainfall in India's changing climate. Their finding stated that climate change is substantially altering the maximum possible precipitation (PMP). Notably, India has experienced a significant increase in PMP since the climate shifted in the 1970s. Wang et al. (2017) investigated whether global warming will drive increasingly severe and frequent extreme climate events. According to their research, Precipitation extremes show higher uncertainty in projections, which increases as global warming exceeds 5 °C. A few studies have also been conducted in different regions of Türkiye (Yavuz and Erdoğan 2012; Tongal 2019; Aksu 2021; Yetik et al. 2024; Kara et al. 2024). For instance, Yeşilırmak and Atatanır (2016) analyzed variations in rainfall intensity and distribution across western Türkiye considering precipitation concentration degree (PCD), precipitation concentration period (PCP), daily precipitation concentration index (DPCI), and monthly precipitation concentration index (MPCI). Their finding was that higher values of the Precipitation Concentration Index (DPCI) were observed in the northwestern and southern parts, indicating these regions experienced more concentrated precipitation. Another study was employed by Koycegiz and Buyukyildiz (2023). They examined rainfall changes in the Seyhan Basin, Türkiye, using advanced statistical techniques.

Despite being surrounded by seas on three sides, Türkiye is not a water-rich country (Gabrielyan 2024). Moreover, Türkiye is characterized by Mediterranean and semi-arid climates (Şan et al. 2024). Agriculture, irrigation, and hydroelectric power generation are of paramount importance in Türkiye. Consequently, precipitation, as a crucial parameter within the hydrological cycle, assumes significant importance. This study investigates the seasonal and annual precipitation characteristics of Türkiye, as well as the spatial and temporal dynamics of precipitation using the Precipitation Concentration Index (PCI) and Seasonality Index (SI). Finally, the influence of the major atmospheric and oceanic indices Pacific Decadal Oscillation (PDO), Atlantic Multidecadal Oscillation (AMO), Nino 3.4, and Southern Oscillation Index (SOI) on precipitation is explored. The novelty of this study lies in its comprehensive regional analysis of Türkiye, considering both two precipitation indices and their relationship with multiple major climatic indices. A comprehensive analysis across all major regions of Türkiye, utilizing both the Precipitation Concentration Index (PCI) and the Standardized Precipitation Index (SI) in conjunction with multiple large-scale climate indices and advanced methods like Cross-Wavelet Transform (XWT), represents a novel undertaking for the country. Consequently, the findings of this study will contribute to a better understanding of precipitation characteristics and their climatic drivers in specific regions of Türkiye.

2 Study area and data

Türkiye, located at the crossroads of Europe and Asia between 36°N and 42°N latitude and 26°E and 45°E longitude, covers a total land area of approximately 780,000 square kilometers. Of this, 97% is situated in Asia and 3% in Europe. The average elevation of Türkiye is 1,130 m, with a gradual increase in altitude from the central part of Anatolia towards the eastern regions. Türkiye is bordered by three seas and has a diverse topography, including lowlands, hills, highlands, and mountains (Deniz et al. 2011). Türkiye 's varied topography, including the Taurus Mountains near the coast, creates distinct regional climates. The mountains act as a barrier, preventing coastal rain clouds from penetrating deep into the country. As a result, most precipitation falls along the coastal areas (Sensoy et al. 2008). The map of Türkiye is shown in Fig. 1. The figure shows seven geographical regions: Marmara, Aegean, Mediterranean, Central Anatolia, Black Sea, Eastern Anatolia, and Southeastern

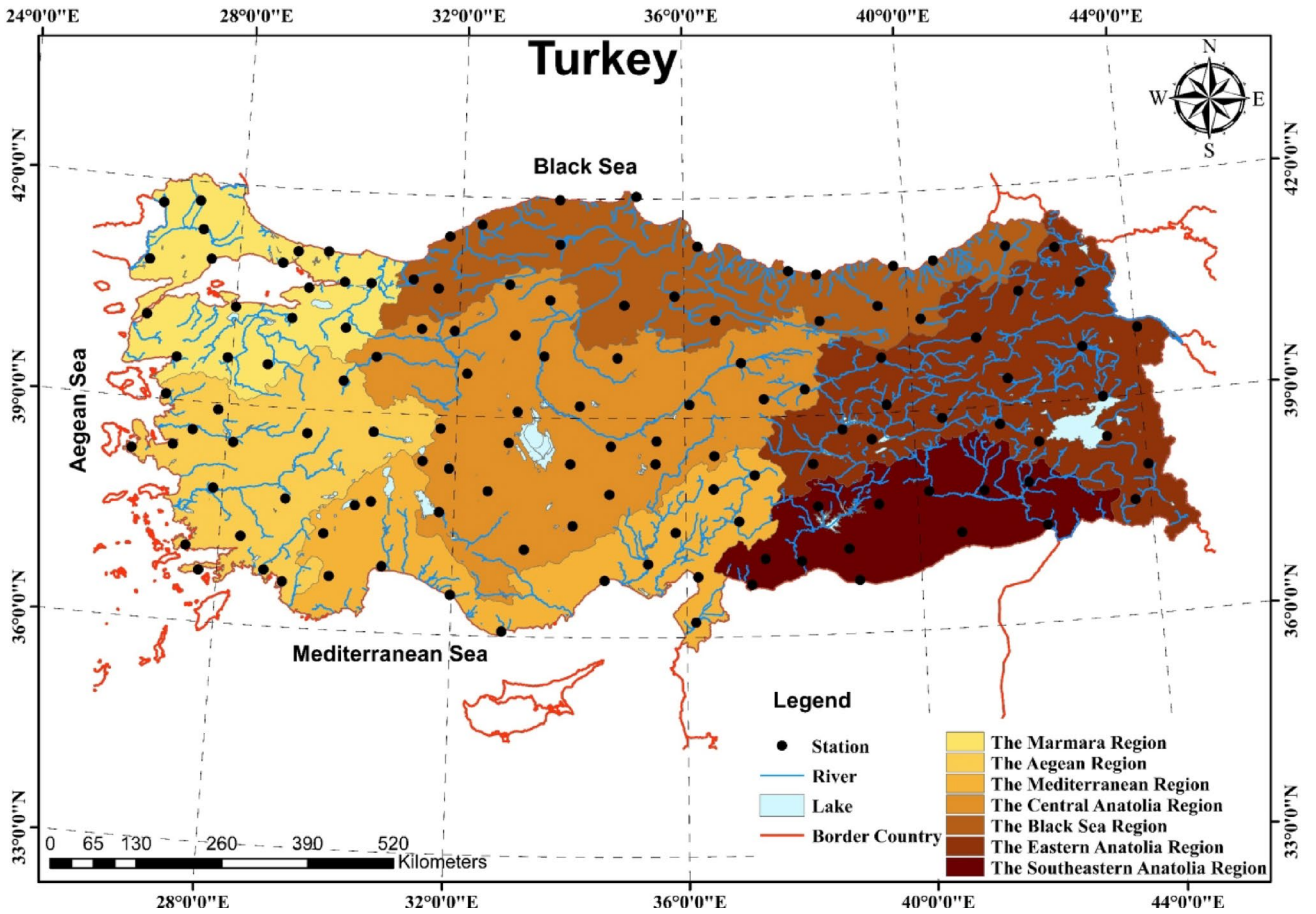

Fig. 1 The distribution of meteorological stations on the Türkiye's map

Table 1 A comprehensive overview of meteorological stations in each region

Regions	Number of stations	Area (km^2)	Mean attitude of stations (m)	Mean annual total precipitation (mm)	Early year of data	Last year of data
Aegean Region	18	79	252.89	660.4	1950	2022
Black Sea Region	19	141	453.42	842.3	1950	2022
Central Anatolia Region	29	151	1061.17	397.4	1950	2022
Eastern Anatolia Region	19	815	1445.37	538.6	1950	2022
Marmara Region	16	67	128.00	671.1	1950	2022
Mediterranean Region	15	110	506.07	709.0	1950	2022
Southeastern Anatolia Region	12	57	654.00	516.4	1950	2022

Anatolia. The study utilized data from 128 meteorological stations from the Turkish State Meteorological Service, with stations representing different regions. Table 1 shows the general descriptive information about the meteorological stations grouped by region. The table provides a comprehensive overview of meteorological stations across various regions in Türkiye. It includes data on the number of stations, the area they cover, their average altitude, annual precipitation, and the earliest and latest years of data available. Most of the stations used in this study are located in the Central Anatolia Region, while the fewest stations in the Southeastern Anatolia Region.

Figure 2 shows the mean annual total precipitation by region in Türkiye from 1970 to 2022, with data for seven different regions. According to the figure, the precipitation patterns vary significantly across the different regions, with some regions experiencing higher overall precipitation levels than others. For example, the Black Sea Region has the highest mean annual precipitation (between 1000 and 1100 mm), while the Central Anatolia Region has the lowest

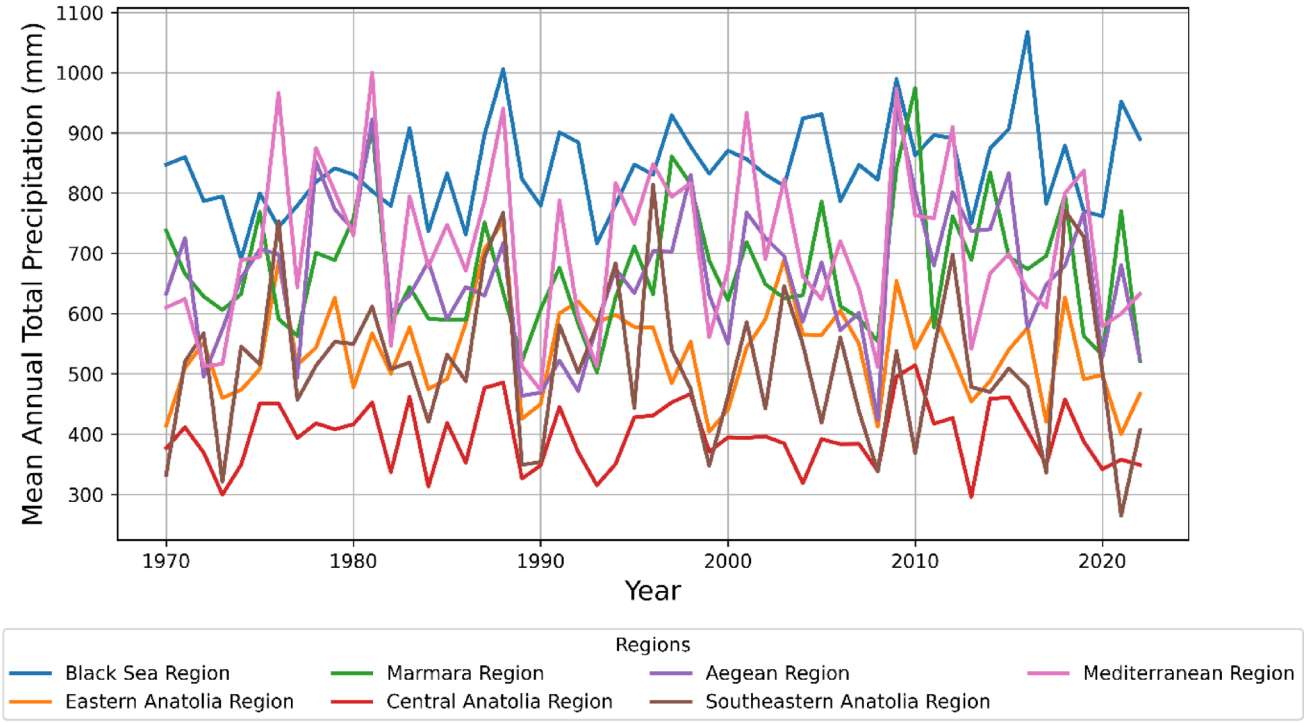

Fig. 2 The average annual total precipitation in each of the seven regions of Türkiye covers the period from 1970 to 2022

(between 500 and 600 mm). There is substantial year-to-year variability in precipitation within each region. For example, the Southeastern Anatolia Region exhibits some of the highest degree of precipitation variability from year to year. The line for this region shows sharp peaks and valleys, with precipitation levels ranging from around 400 mm to over 900 mm within the span of just a few years. This suggests a highly variable precipitation regime in this region. In contrast, the Central Anatolia Region displays a relatively more stable precipitation pattern over time, with the line showing smaller deviations from the mean compared to regions like Southeastern Anatolia.

3 Methodology

3.1 Precipitation concentration index (PCI)

To quantify monthly precipitation variability, this study employed the Precipitation Concentration Index (PCI), originally proposed by Oliver (1980) and widely used (e.g., Luis et al. (1997). The annual PCI was evaluated using Eq. (1).

$$PCI = 100 \times \frac{\sum_{i=1}^{12} P_i^2}{\left(\sum_{i=1}^{12} P_i\right)^2} \tag{1}$$

where P_i denotes the monthly precipitation recorded at each meteorological station for a spesific month (i) within a given year. Generally, regions with lower annual precipitation tend to experience greater variability in monthly rainfall. As a result, higher PCI values indicate a greater concentration (unevenness) of precipitation within the year, with a larger proportion of the total rainfall occurring in a shorter period (Oliver 1980). To analyze seasonal precipitation patterns, the PCI (seasonal) was calculated for each season (spring (MAM), summer (JJA), autumn (SON), and winter (DJF) using Eqs. (2),

$$\text{PCI (seasonal)} = 25 \times \frac{\sum_{i=1}^{3} P_i^2}{\left(\sum_{i=1}^{3} P_i\right)^2} \tag{2}$$

Following Oliver's classification (1980), PCI seasonal values between 8.3 and 10 indicate uniform monthly precipitation distribution, 10 to 15 suggest moderate concentration, 15 to 20 denote irregular seasonal distribution, and values above 20 signify highly irregular precipitation patterns (Darand and Pazhoh 2022). To assess the relative variability of annual precipitation, the coefficient of variation (CV) was calculated for each station, representing the annual total precipitation as a percentage of the mean ($CV = (Std\,Dev/Mean) * 100\%$).

3.2 Seasonality index (SI)

The precipitation seasonality index (Walsh and Lawler 1981) was quantify the degree of seasonal variation in long-term mean monthly precipitation. Table 2 shows the classification of SI. The index is defined as follows:

$$SI = \frac{1}{\bar{R}} \sum_{n=1}^{12} \left| \bar{X}_n - \frac{\bar{R}}{12} \right| \tag{3}$$

where $\bar{R}$ denotes annual mean precipitation, and $\bar{X}_n$ represents the mean precipitation of month n.

3.3 Mann-Kendall (MK) trend test and sens's slope estimator

The Mann-Kendall trend test (Mann 1945; Kendall 1975) assesses the presence of a monotonic trend in a time series (Annual total precipitation) by examining the correlation between the ranks of data points. For a given time series {Xi, i = 1, 2, …, n}, the null hypothesis H0 assumes no trend, while the alternative hypothesis H1 suggests a monotonic trend. The test statistic S is calculated as follows:

$$S = \sum_{k=1}^{n-1} \sum_{j=k+1}^{n} sgn\left(x_j - x_k\right) \tag{4}$$

where n represents the number of the data, t_i is noted as the length of the tied rank group and x_j and x_k represent the data point in years j and k (j > k).

$$sgn\left(x_j - x_k\right) = \begin{cases} 1 & \left(x_j - x_k\right) > 0 \\ 0 & \left(x_j - x_k\right) = 0 \\ -1 & \left(x_j - x_k\right) < 0 \end{cases} \tag{5}$$

$$Var\left(S\right) = \frac{n\left(n-1\right)\left(2n+5\right) - \sum_i^r t_i\left(t_i-1\right)\left(2t_i+5\right)}{18} \tag{6}$$

Table 2 The classification of the seasonality index (Walsh and lawler 1981)

SI	Precipitation regimes
≤ 0.19	Precipitation spread throughout by the year (very equable)
0.20–0.39	Equable but with a definite wetter season
0.40–0.59	Rather seasonal with a short drier season
0.60–0.79	Seasonal
0.80–0.99	Markedly seasonal with a long dry season
1.00–1.19	Most precipitation in < 3 months
≥ 1.20	Extreme seasonality, with almost all precipitation in 1–2 months

$$Z = \begin{cases} \dfrac{S-1}{\sqrt{Var\left(S\right)}} & S > 0 \\ 0 & S = 0 \\ \dfrac{S+1}{\sqrt{Var\left(S\right)}} & S < 0 \end{cases} \tag{7}$$

The test statistic, Z, follows a standard normal distribution with a mean of 0 and a standard deviation of 1 under H. The null hypothesis (H0) states that there is no significant trend, while the alternative hypothesis (H1) suggests a significant trend. In a two-tailed test, H0 and H1 are evaluated at different significance levels (α). For α = 10%, Z = ± 1.645; for α = 5%, Z = ± 1.96; and for α = 1%, Z = ± 2.57 (Ali et al. 2019; Esit 2022).

Sen's slope (Sen 1968) is evaluated as

$$S_i = median\left(\frac{\left(Y_j - Y_k\right)}{j-k}\right) \; for \; i = 1, 2, 3 \ldots N\left(j > k\right) \tag{8}$$

where Y_j and Y_k denote as times j and k. The median of the $N = \frac{n(n-1)}{2}$ which n is the number of the time periods.

3.4 Pearson correlation and cross-correlation analysis

The Pearson correlation coefficient (r) was employed to examine the simultaneous relationship between precipitation and the oceanic-atmospheric circulation patterns. The Pearson correlation coefficient (Benesty et al. 2009) measures the linear association between series x and y. The coefficient r is determined by the following formula:

$$r = \frac{\sum_{i=1}^{n}\left(X_i - \bar{X}\right)\left(Y_i - \bar{Y}\right)}{\sqrt{\sum_{i=1}^{n}\left(X_i - \bar{X}\right)^2}\sqrt{\sum_{i=1}^{n}\left(Y_i - \bar{Y}\right)^2}} \tag{9}$$

Xi and *Yi* represent the precipitation and ocean-atmospheric circulation indices, respectively, where i denotes the individual data point. $\bar{X}$ and $\bar{Y}$ are the mean values of *Xi* and *Yi*. The correlation coefficient, r, ranges from − 1 to 1. A positive r ($r > 0$) indicates a positive relationship, while a negative r ($r < 0$) indicates a negative relationship (Zhang et al. 2013).

Cross-correlation function (CCF) analyzes the similarity between two-time variables over time, accounting for time lags. This method reveals how one variable correlates with past values of another, providing a more comprehensive understanding of their relationship compared to simple correlation, which only considers contemporaneous values (Rahmani and Fattahi 2021). The CCF is determined by the following formula:

$$r_k = \frac{\hat{C}_K(x,y)}{\hat{\delta}_x \hat{\delta}_{y+k}} \tag{10}$$

the sample covariance is noted by $\widehat{C}_K$(x, y), and the sample mean square deviations, $\widehat{\delta}_x$ and $\widehat{\delta}_{y+k}$, are evaluated as follows:

$$\begin{cases} \hat{C}_K = \dfrac{1}{n-k}\displaystyle\sum_{i=1}^{n-k}(x_i-\bar{x})(y_{i+k}-\bar{y}_{i+k}) \\ \hat{\delta}_x = \left[\dfrac{1}{n-k}\displaystyle\sum_{i=1}^{n-k}(x_i-\bar{x})^2\right]^{\frac{1}{2}} \\ \hat{\delta}_{y+k} = \left[\dfrac{1}{n-k}\displaystyle\sum_{i=1}^{n-k}(y_{i+k}-\bar{y}_{i+k})^2\right]^{\frac{1}{2}} \end{cases} \tag{11}$$

3.5 Cross-wavelet transform (XWT)

XWT is a method for measuring the joint variability of two signals across time and frequency (Torrence and Webster 1998; Torrence and Compo 1998). Wavelet coherence is calculated by first determining the wavelet transforms of time series x(t) and y(t), resulting in Wx(s, τ) and Wy(s, τ), and then computing the cross-wavelet transform using the equation (Grinsted et al. 2004):

$$W_{x,y}(s,\tau) = W_x(s,\tau)\, W_y^*(s,\tau) \tag{12}$$

where * shows complex conjugation. The wavelet coherence of the time series x(t) and y(t), given their wavelet spectra Wx(s, τ) and Wy(s, τ), and cross-wavelet spectrum Wx, y(s, τ), is determined by the equation (Grinsted et al. 2004; Rouyer et al. 2008):

$$R_{x,y}^2(s,\tau) = \frac{\left|\left\langle s^{-1} W_{x,y}(s,\tau)\right\rangle\right|^2}{\left\langle s^{-1}\left|W_x(s,\tau)\right|^2\right\rangle \left\langle s^{-1}\left|W_y(s,\tau)\right|^2\right\rangle} \tag{13}$$

The smoothing operation <…> is applied to both time τ and scale s, and the squared wavelet coherence $R_{x,y}^2(s,\tau)$ lies within the interval [0, 1].

3.6 Climate indices

The chosen climate indices represent simultaneous fluctuations in climate anomalies across extensive regions. For instance, the AMO index quantifies the oscillation of sea surface temperatures in the North Atlantic. This climate oscillation has a periodic nature, with a cycle time of 60 to 80 years, and each cycle transitioning between warm and cool phases (Schlesinger and Ramankutty 1994; Abdelkader and Yerdelen 2022). Due to its widespread impact on the Northern Hemisphere, AMO was considered in this research. Several studies have identified a strong relationship between AMO fluctuations and precipitation patterns in various regions of the Northern Hemisphere (Martin and Thorncroft 2014; Tao et al. 2021; Gu and Adler 2023). The El Niño-Southern Oscillation (ENSO) is a dominant mode of interannual climate variability originating in the tropical Pacific Ocean. This study uses the Nino 3.4 index to represent ENSO. The Nino 3.4 index reflects SST anomalies in the central equatorial Pacific (5°N-5°S, 170°W-120°W) and is widely used to monitor ENSO events. The ENSO cycle alternates between two phases: El Niño, associated with warming, and La Niña, associated with cooling (Ropelewski and Halpert 1986; Dai and Wigley 2000).

The PDO is a cyclical climate pattern in the mid-latitude Pacific Ocean, involving interactions between the ocean and atmosphere. Extreme PDO events influence the climate of the Pacific Ocean and North America, and, along with ENSO, are influenced by sea surface temperature anomalies (Mantua et al. 1997). The Southern Oscillation Index (SOI) is calculated as the difference in sea level pressure between Tahiti and Darwin, two locations in the Eastern and Western Pacific, respectively. This atmospheric pressure pattern is a common indicator of El Niño and La Niña events, which influence weather patterns in the Indo-Australian region (Wu et al. 2022). The climate indices employed in this study, along with their associated data, were obtained from the NOAA Physical Sciences Laboratory (PSL) (link: https://psl.noaa.gov/data/climateindices/list/).

4 Results

4.1 Assessment of precipitation variability

Initially, Monthly precipitation data from 128 stations were selected from an initial pool of 150 based on stringent quality and homogeneity criteria, including a minimum record length of 40 years, less than 10% missing data, and passing the SNHT (Standard Normal Homogeneity Test) for homogeneity. This selection process was applied to data spanning the period 1950–2022. Missing data were imputed using arithmetic mean interpolation. Following these procedures, the spatial distribution of precipitation across Türkiye, on both seasonal and annual scales, is presented in Fig. 3. These maps are generated using the IDW (Inverse Distance Weighted) method in ArcGIS. According to Fig. 3, the annual precipitation map reveals significant spatial heterogeneity across the country. Coastal regions, particularly the Black Sea coast in the north and the Mediterranean coast in the south, exhibit markedly higher annual precipitation totals,

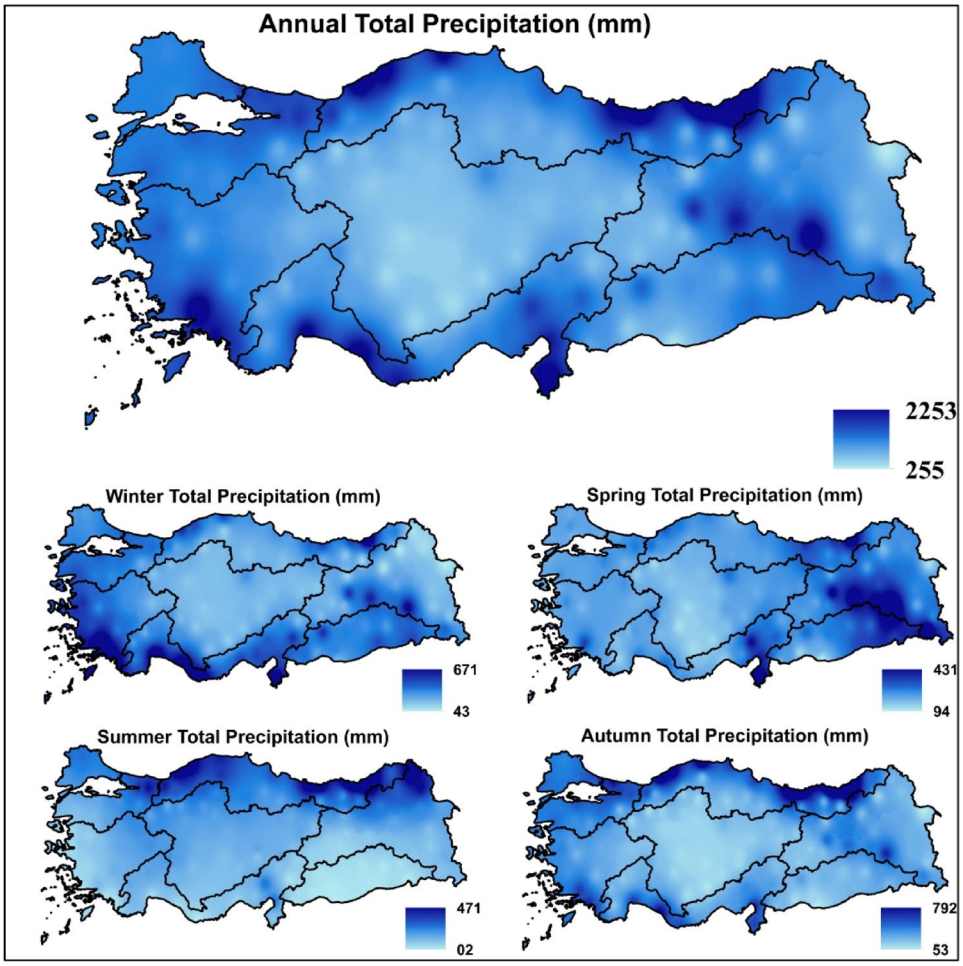

Fig. 3 The spatial distribution of annual and seasonal total precipitation across Türkiye. The blue color scale, ranging from darker to lighter shades, indicates increasing precipitation levels

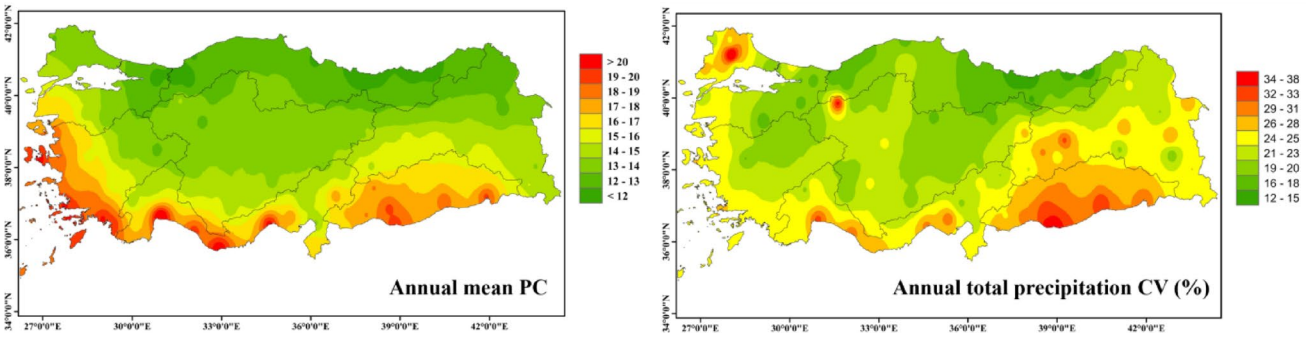

Fig. 4 The spatial distribution of the annual mean PC (left) and annual total precipitation coefficient of variance (right)

with some areas receiving up to 2000 mm. In contrast, central Anatolia displays considerably lower (< 300 mm) precipitation, indicating a more arid climate. Winter precipitation is highest along the western and southern coasts, likely due to maritime influences. Spring precipitation shows a more uniform distribution, with elevated levels in the northeastern regions. Summer precipitation exhibits a stark north-south gradient, with the Black Sea coast receiving substantially more rainfall than the southern regions. Autumn precipitation patterns resemble the annual distribution, with coastal areas receiving higher totals than inland regions. This spatial and temporal analysis of precipitation patterns is crucial for understanding regional water resources, agricultural potential, and ecological dynamics in Türkiye. These results are convenient with Yavuz and Erdoğan (2012), Yetik et al. (2024).

Figure 4 shows the spatial distribution of the annual mean PC and annual total precipitation coefficient of variance (CV%) over Türkiye. The PC index map shows a clear north-south gradient in precipitation concentration.

Northern regions, particularly the Black Sea coast, exhibit lower PC values (< 12–13), indicating a more uniform distribution of precipitation throughout the year. In contrast, southern and western coastal areas show higher PC values (> 18), with some regions exceeding 20. This suggests that these areas experience more concentrated periods of rainfall. The CV map reveals the relative variability of annual precipitation totals. Higher CV values indicate greater year-to-year variability in total precipitation. The map shows that coastal regions, especially in the south and southeast, have higher CV values (> 29%), with some areas exceeding 34%. Central and northern regions generally show lower CV values (< 23%), indicating more consistent annual rainfall totals. Coastal areas, particularly in the south and west, show both high PC and high CV values. This suggests these regions not only have more concentrated rainfall periods but also experience greater interannual variability in total precipitation. The Black Sea coast shows low PC values but moderate CV values, indicating consistent year-round precipitation but moderate interannual variability. Central Anatolia shows moderate PC values and relatively low CV values, suggesting a balance between seasonal concentration and year-to-year consistency in precipitation. Our findings are consistent with previous studies (Mrad et al. 2019; Boughdadi et al. 2024).

Figure 5 indicates the spatial distribution of seasonal PC index over Türkiye. *Winter*: PC values show a heterogeneous distribution with values ranging from 37 to 44. Higher PC values (depicted in orange and red) are observed in the western coastal regions and parts of southeastern Türkiye, indicating more concentrated precipitation patterns. The Black Sea coast and central Anatolia exhibit lower PC values (green areas), suggesting more uniform winter precipitation distribution in these regions. *Spring*: PC values range from 37 to 54, showing the highest variability among all seasons. The southern and southwestern coastal areas display notably high PC values, implying concentrated spring rainfall events. In contrast, northern and central regions show lower PC values, indicative of more evenly distributed spring precipitation. *Summer*: PC values reveals the most pronounced concentration patterns, with values ranging from 39 to 96. Extremely high PC values are evident in southern and southeastern Türkiye, suggesting highly concentrated and possibly intense summer precipitation events in these areas. The northern regions, particularly the Black Sea coast, maintain lower PC values, indicating more consistent summer rainfall patterns. *Autumn*: PC values range from 38 to 69, showing a pattern somewhat similar to spring but with generally higher values. The southern coastal regions and southeastern Türkiye exhibit high PC values, while the northern and central areas display moderate to low values.

Figure 6 indicates A decadal analysis of the Precipitation Concentration Index (PCI) in Türkiye from 1980 to 2020, examining the PCI trends in four distinct decades: 1980–1990, 1990–2000, 2000–2010, and 2010–2020. *1980–1990*: This decade shows a distinct spatial pattern with high PCI values (20–25) along the western and southern coasts, indicating highly concentrated precipitation in these regions. The central and eastern parts of Türkiye exhibit lower PCI values (10–15), suggesting more evenly distributed

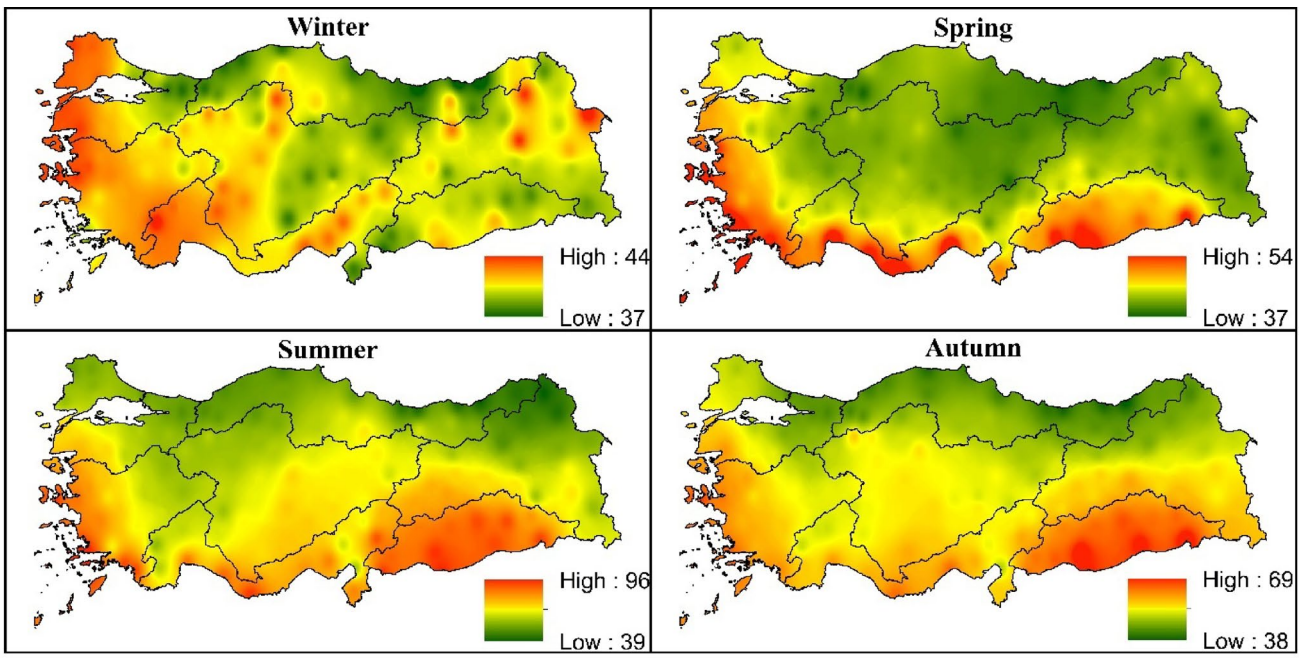

Fig. 5 A comprehensive spatial analysis of the seasonal Precipitation Concentration (PC) index across Türkiye

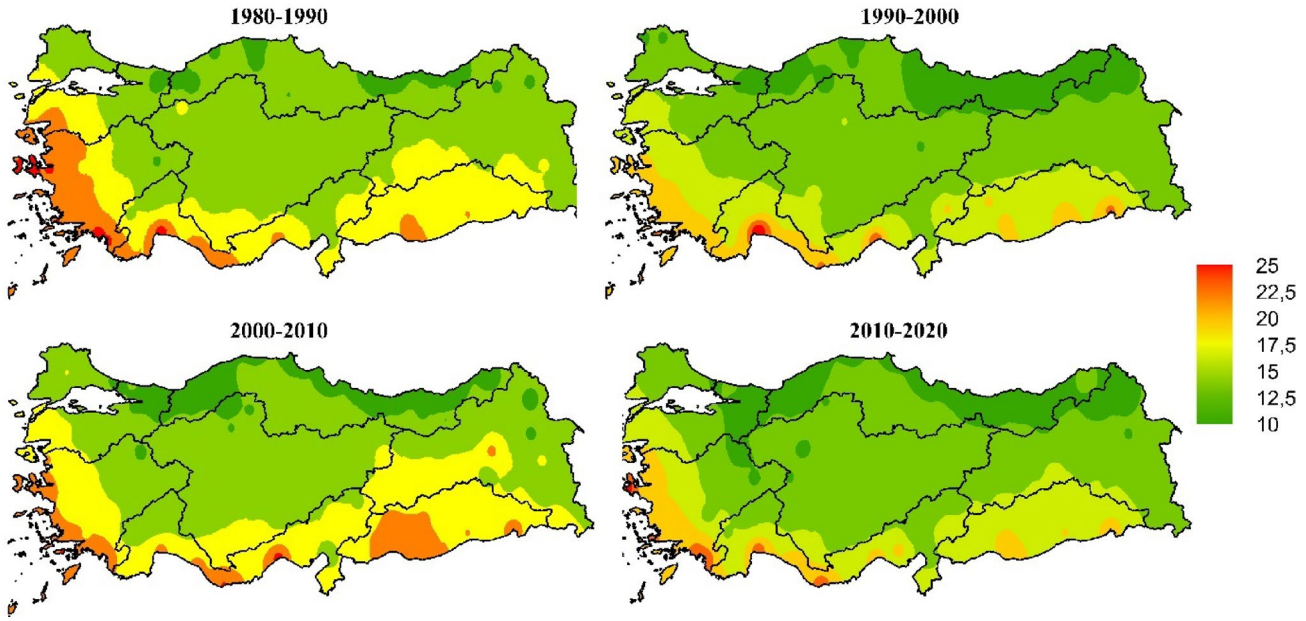

Fig. 6 The decadal analysis of the Precipitation Concentration Index (PCI) across Türkiye from 1980 to 2020, divided into four distinct (1980–1990, 1990–2000, 2000–2010 and 2010–2020) decades

precipitation. *1990–2000*: Compared to the previous decade, there's a noticeable reduction in PCI values across much of the country. The western coastal areas maintain relatively high PCI values, but the extent of the highest concentration areas has decreased. The central and eastern regions show a slight increase in PCI values, indicating a trend towards more concentrated precipitation patterns in these areas. *2000–2010*: This decade exhibits a partial return to patterns similar to the 1980s, with increased PCI values in the southwestern coastal areas. However, the central and northern regions maintain lower PCI values compared to the 1980s. A notable feature is the emergence of higher PCI values in the southeastern region, suggesting an increase in precipitation concentration in this area. *2010–2020*: The most recent decade shows a further moderation of PCI values across much of Türkiye. While the southwestern coast still maintains higher PCI values, they are less intense compared to previous decades. The central and northern regions continue to show relatively low PCI values, indicating more uniform precipitation distribution.

Figure 7 shows the spatial distribution of SI across Türkiye based on annual and seasonal scales. The annual SI reveals a pronounced north-south gradient across Türkiye. The northern regions, particularly the Black Sea coast, exhibit low SI values (0.79-1.0), indicating relatively uniform precipitation distribution throughout the year. In stark contrast, the southern and southeastern regions display high SI values (up to 1.78), suggesting a strong seasonality in precipitation patterns. Central Anatolia shows intermediate values, representing a transition zone between these two distinct regimes. The winter SI shows high values (0.85-1.0) along the western and southern coasts, indicating concentrated winter precipitation in these Mediterranean climate-influenced areas. The eastern and northeastern regions display lower SI values, suggesting more evenly distributed winter precipitation. The spring SI values are generally lower compared to winter, ranging from 0.52 to 1.24. The southern coastal areas maintain higher SI values, while northern and central regions show lower values, indicating a more uniform distribution of spring precipitation across much of the country. The summer SI map reveals the most pronounced spatial variability. Extremely high SI values (up to 1.83) are observed in the southern and southeastern regions, indicating highly concentrated summer precipitation events. In contrast, the Black Sea coast and parts of northeastern Türkiye exhibit low SI values, suggesting more consistent summer rainfall patterns. Autumn SI patterns are similar to spring but with generally higher values, ranging from 0.57 to 1.69. The southern coastal regions and southeastern Türkiye show high SI values, while the northern areas display lower values, indicating more uniform autumn precipitation distribution.

4.2 Trend and sen's slope results

Figure 8 represents the spatial distribution results of Mann-Kendall (MK) and Sen's slope tests for the annual mean Precipitation Concentration Index (PCI) across the country. The MK results illustrate the z-scores from the Mann-Kendall test, which indicates the presence and strength of

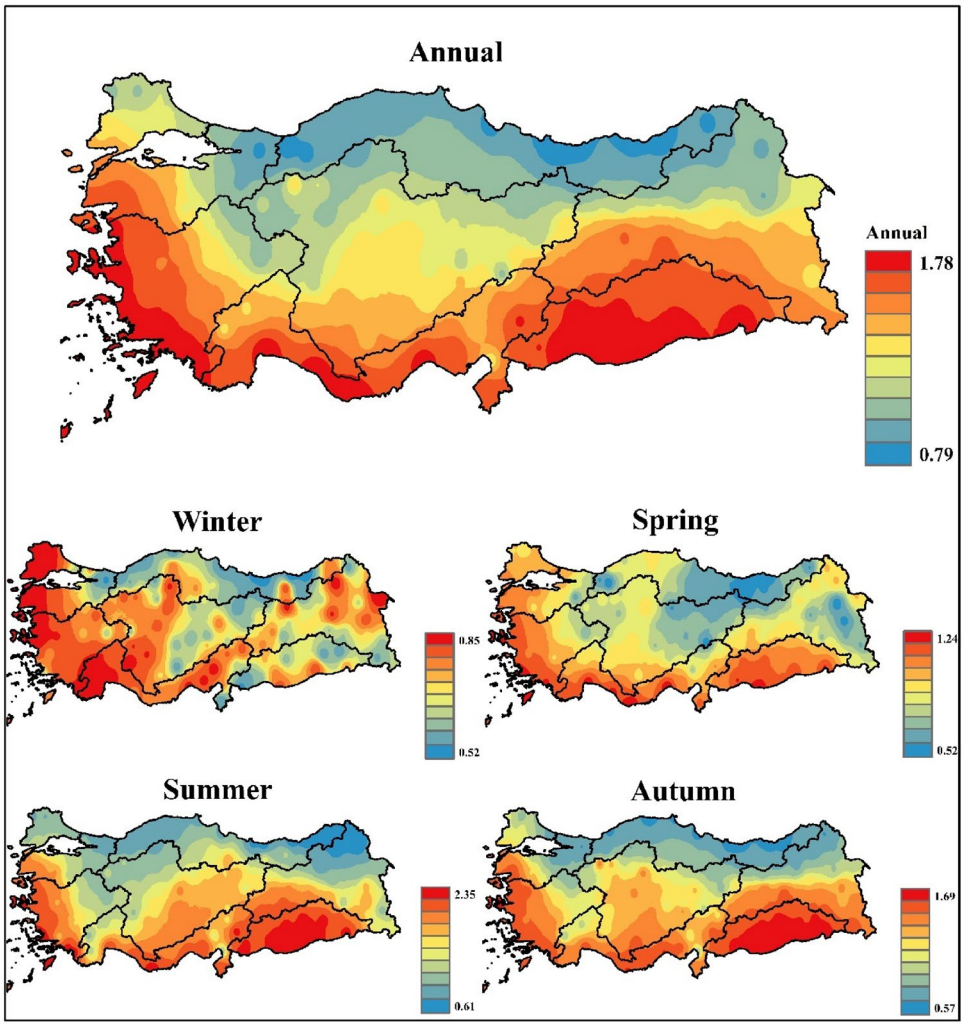

Fig. 7 The analysis of the Seasonality Index (SI) across Türkiye considering both annual and seasonal scales

monotonic trends in the PCI data. The color-coded legend ranges from blue (positive z-scores) to red (negative z-scores), with varying intensities representing different ranges of statistical significance. Regions with strong positive trends are scattered throughout the country, particularly notable in some northern and eastern areas. Negative trends of varying intensities are observed in numerous locations, with some clustering in the western and southern coastal regions. However, a few stations indicate a decreasing or increasing trend at a significant level. Sen's slopes quantify the magnitude of PCI change per unit time. The legend indicates slope values ranging from − 0.04 to 0.04, with darker blue shades representing more negative slopes and lighter shades indicating more positive slopes. The southeast and along certain coastal areas exhibit negative slopes (-0.04 to -0.01), indicating a trend towards more uniform precipitation distribution over time.

4.3 The effects of atmospheric-ocean indices over precipitation variability

This part employs Cross-wavelet and Pearson correlation analyses to examine how atmospheric-oceanic indices affect precipitation across Türkiye and its regions. First, Figs. 9 is created for the same year and one year lagged between the selected climate indices and precipitation data. In this way, it was investigated whether the effects of climate indices were effective in subsequent years.

The AMO exhibits a heterogeneous correlation pattern with precipitation across Türkiye. The southeastern and coastal regions show predominantly negative correlations (blue areas), while central and northern regions display positive correlations (yellow to red areas). The lagged correlation map shows a notable shift towards more widespread negative correlations, particularly in the western and southeastern regions. This suggests a potential delayed influence of the AMO on Turkish precipitation patterns, with increased predictive power for certain areas.

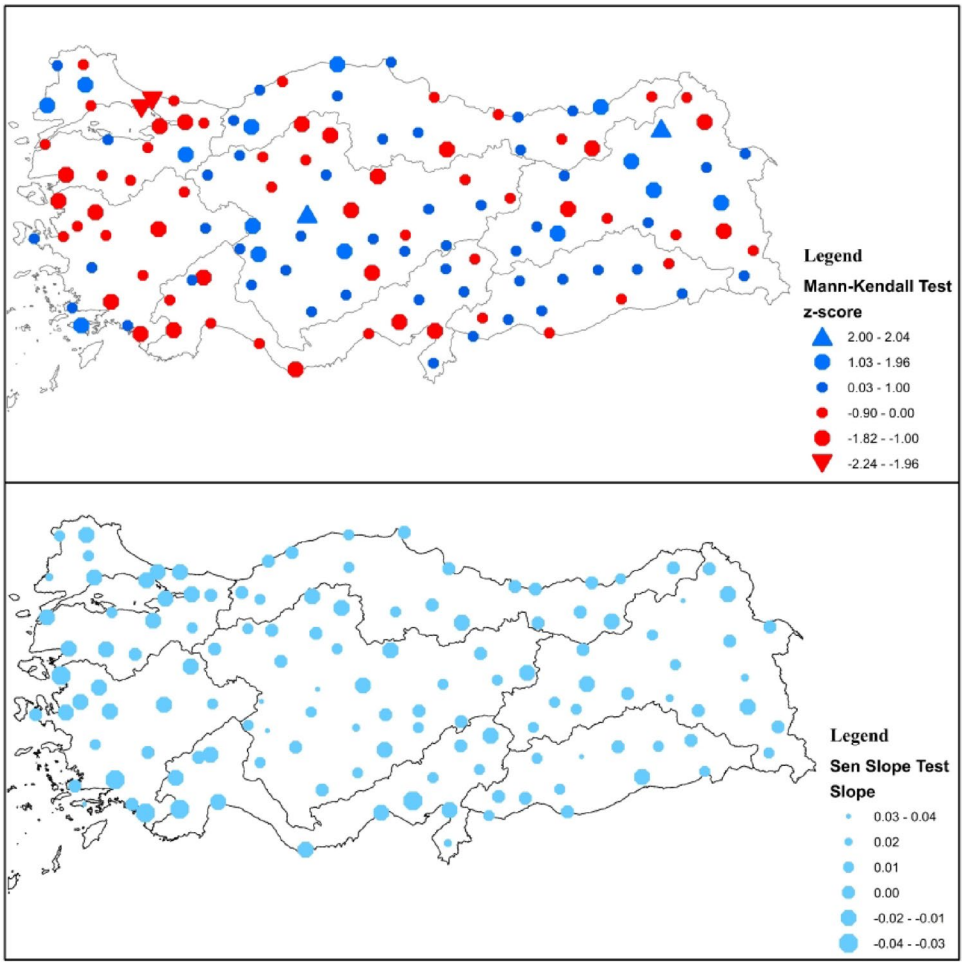

Fig. 8 The Mann-Kendall trend test and Sen's slope results of annual mean PC indices across Türkiye

The PDO demonstrates strong positive correlations across much of Türkiye, particularly in central and eastern regions. The pattern is more uniform than the AMO, with numerous significant correlations, indicating a robust contemporary relationship between the PDO and Turkish precipitation. The lagged correlations for PDO show a weakening of the relationship, with lower correlation values and fewer significant areas.

Nino 3.4 exhibits strong positive correlations in the eastern half of Türkiye, with significant values concentrated in this region. The western areas show weaker or slightly negative correlations, highlighting a clear east-west gradient in the ENSO influence on Turkish precipitation. The lagged correlation map for Nino 3.4 shows a substantial relationship weakening, with much lower correlation values and very few significant areas.

The SOI correlation pattern is generally weak and mixed across Türkiye, with small patches of positive and negative correlations. Few areas show significant correlations, indicating a less pronounced direct influence of SOI on Turkish precipitation compared to the other indices. Interestingly, the lagged correlation map for SOI shows some intensification of correlations, particularly positive correlations in the northwest are observed.

Generally, the same-year correlations are stronger and more extensive than the one-year-ahead correlations for AMO, PDO, and Nino 3.4. This indicates that these indices have more immediate influences on Türkiye precipitation.

Figure 10 shows cross-correlation analyses between regional precipitation and four major climate indices (AMO, Nino3.4, PDO, and SOI) for seven distinct regions of Türkiye : Aegean, Black Sea, Central Anatolia, Eastern Anatolia, Marmara, Mediterranean, and Southeastern Anatolia. The analysis spans a range of lead/lag times from − 50 to + 50 months, allowing for the examination of both lead and lag relationships between climate indices and regional precipitation. Aegean Region: Shows strong oscillatory patterns for all indices, with AMO having the most pronounced effect. Black Sea Region: Exhibits smoother correlation patterns, with AMO dominating. Pacific indices (Nino3.4, PDO) show weaker correlations compared to other regions. AMO (red line) generally shows the highest amplitude of correlation across most regions, indicating its strong influence on the Türkiye precipitation series. However, SOI (purple

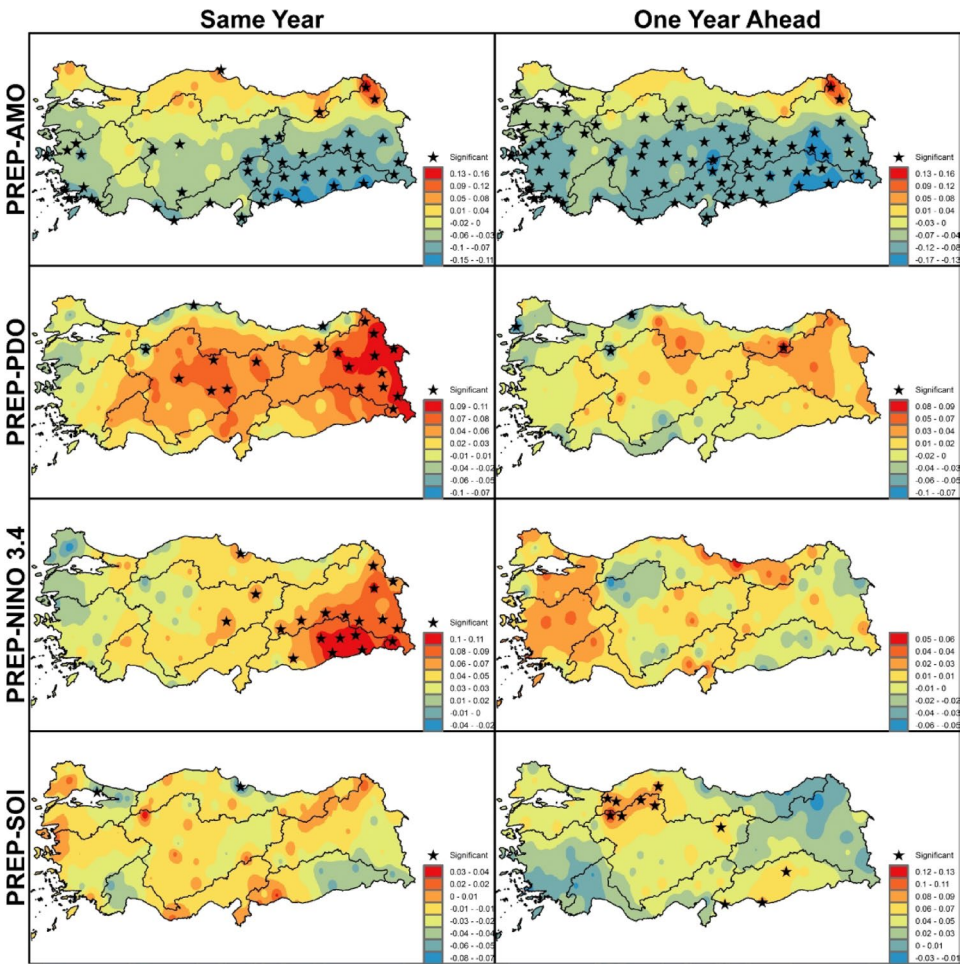

Fig. 9 Pearson correlations between precipitation and four major climate indices: AMO, PDO, Nino 3.4, and SOI for both concurrent (same year) and lagged (one year ahead)

line) shows weaker correlations compared to other indices. Coastal regions (Aegean, Black Sea, Mediterranean) generally show stronger correlations with AMO, likely due to the Atlantic influence on Mediterranean climate systems.

Figure 11 indicates the results of cross-wavelet transform (XWT) analyses between regional precipitation patterns in Türkiye and three major climate indices: AMO, Nino3.4, and PDO. The analyses cover seven distinct regions of Türkiye from 1970 to 2020, providing insights into the time-frequency relationships between local precipitation and large-scale climate patterns. According to the results: *The Marmara Region*: Shows strong coherence with AMO at longer periodicities (8–16 years), with arrows predominantly pointing right-down, indicating an in-phase relationship with precipitation slightly lagging AMO by approximately 45°. Nino3.4 exhibits significant coherence at the 2–4 year band around 1990–2000, with arrows pointing left, suggesting an anti-phase relationship where El Niño events correspond to decreased precipitation. *Mediterranean Region*: Demonstrates consistent coherence with AMO at decadal scales with arrows pointing right, indicating an in-phase relationship where positive AMO phases are associated with increased precipitation. Notable interactions with Nino3.4 at interannual scales (2–4 years) show arrows pointing left-up, suggesting an anti-phase relationship with precipitation slightly leading Nino3.4. *Southeastern Anatolia Region*: Exhibits strong coherence with PDO, particularly at longer periodicities (8–16 years), with arrows predominantly pointing left, indicating an anti-phase relationship where positive PDO phases correspond to decreased precipitation in this region. *Aegean Region*: Shows diverse interactions across all indices. With PDO, significant coherence at the 8-year band shows arrows pointing left-down, suggesting an anti-phase relationship with precipitation lagging PDO. *Central Anatolia Region*: Demonstrates complex patterns of coherence, particularly with Nino3.4 and PDO. The significant coherence with Nino3.4 at the 2–4 year band around 2000–2010 shows arrows pointing predominantly left, indicating an anti-phase relationship. *Black Sea Region*: Exhibits strong coherence with AMO at longer periodicities with arrows pointing right, indicating an in-phase relationship where positive AMO phases correspond to increased precipitation. Relationships with Pacific indices show more variable phase angles across different time periods. *Eastern*

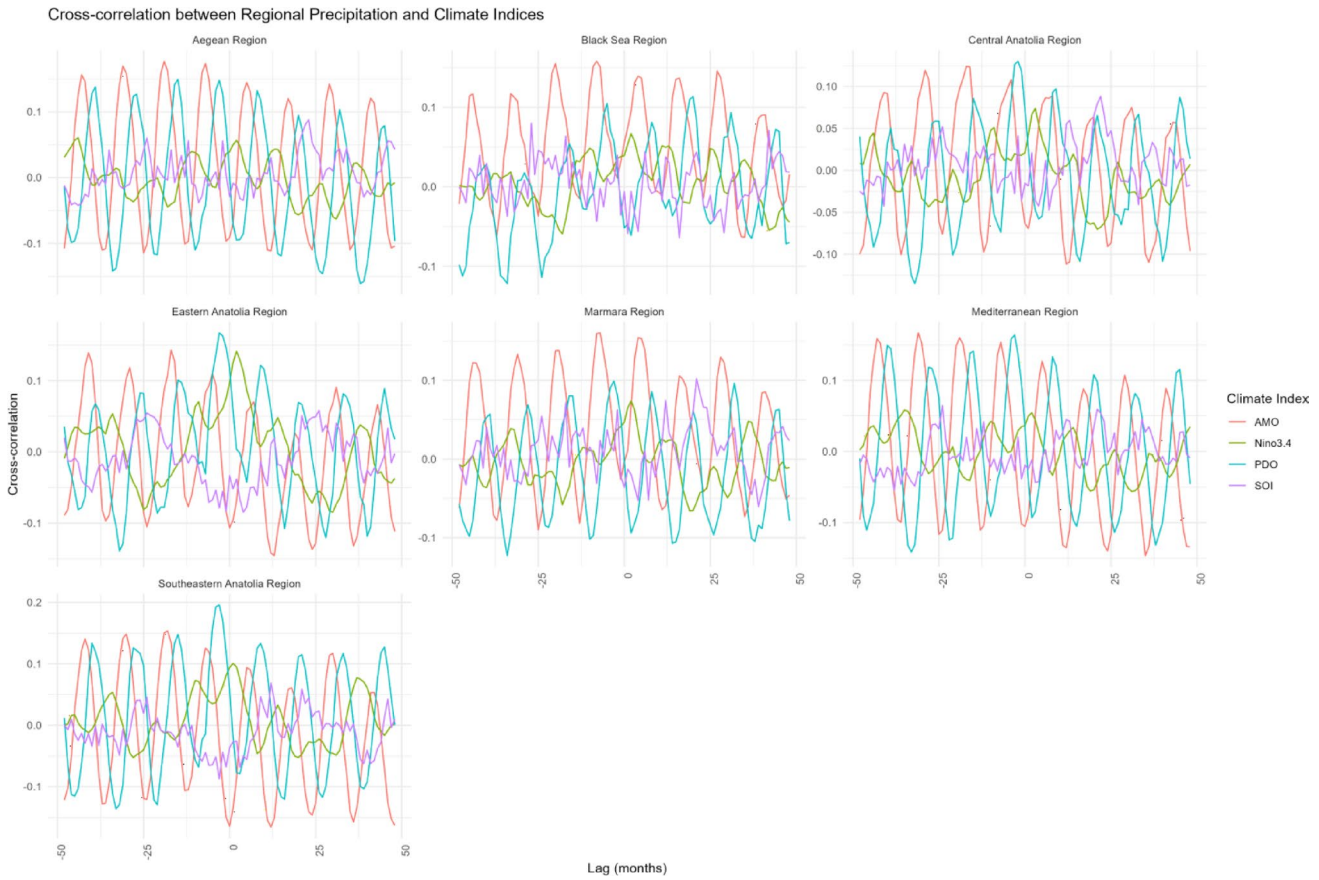

Fig. 10 Cross-correlation between monthly mean precipitation and climate indices for each region across Türkiye

Anatolia Region: Shows distinct patterns of coherence with all indices, robust with AMO at decadal scales with arrows pointing predominantly right-up in significant regions, suggesting an in-phase relationship with precipitation slightly leading AMO.

AMO shows stronger and more consistent coherence at longer periodicities (16+ years) across most regions, generally with in-phase relationships, indicating its importance in positively modulating long-term precipitation trends in Türkiye. In contrast, Pacific indices (ENSO and PDO) tend to show more anti-phase relationships, particularly in southern and central regions. Many areas show shifts in coherence patterns over time, particularly evident in the post-2000 period, which may indicate changing climate dynamics or teleconnection patterns affecting precipitation in Türkiye.

5 Discussion

This study has provided a comprehensive analysis of Türkiye's precipitation dynamics, revealed significant spatial and temporal heterogeneity and highlighted the influence of key atmospheric-ocean interactions. The observed spatial patterns, with higher annual precipitation concentrated along the Black Sea and Mediterranean coasts and a distinct north-south gradient in summer precipitation, corroborate findings from previous climatological studies (Baltacı et al. 2018; Sezen and Partal 2019üşcü and Aksoy 2024). For example, Kömüşcü and Aksoy (2024) studied on the spatial variability of Turkey's annual and seasonal precipitation. According to their results show that Turkey's annual precipitation for the 1991–2020 climatological normal period averages 574 mm, with approximately 70% occurring during the wet season (October to May). Precipitation exhibits geographic variability, with sharp contrasts between coastal and inland areas—from just 300 mm in central Anatolia to over 2,000 mm along the eastern Black Sea coast. Our analysis extends these observations by quantifying regional differences in precipitation regimes through the Precipitation Concentration (PCI) and Coefficient of Variation (CV) indices. The high seasonal concentration and interannual variability identified in the southern and western coastal regions likely reflect the dominant influence of episodic Mediterranean cyclones, characterized by intense precipitation events concentrated within shorter periods. Conversely, the more uniform year-round precipitation along the Black

Fig. 11 Cross-wavelet analysis between regional precipitation and climate indices (AMO, PDO, and Nino3.4) across Türkiye

Sea coast suggests a more consistent moisture supply from the Black Sea and a less pronounced influence of extreme seasonal variations.

The observed dominance of same-year correlations over one-year-ahead correlations for AMO, PDO, and Nino 3.4 indicates that these ocean-atmosphere indices have a more immediate and direct influence on Türkiye's precipitation patterns, particularly at seasonal to interannual timescales. However, the presence of lagged effects—especially for AMO and SOI—points to the complexity and temporal variability in these teleconnections, suggesting that both short-term and delayed climatic signals should be considered when evaluating hydroclimatic responses. The Cross-Wavelet Transform analysis reveals that AMO plays a dominant role in modulating long-term precipitation variability, especially in the Mediterranean and Eastern Anatolia regions, while the PDO's influence is more pronounced in Southeastern Anatolia. These regional differences highlight the spatially heterogeneous nature of teleconnection impacts and the importance of localized climate assessments.

Furthermore, the post-2000 shifts in coherence patterns across many regions suggest that teleconnection behavior is evolving—likely influenced by broader changes in global climate dynamics—underscoring the need for adaptive strategies in climate modeling, water resource planning, and drought management across Türkiye. Moreover, our study and Unal et al. (2012) and Kömüşcü and Aksoy (2024) indicates that the AO index exhibited the strongest correlation with precipitation patterns across Turkey compared to the other teleconnection indices examined.

This study is not without limitations. The analysis relies on historical observational data, and longer time series could provide a more robust assessment of long-term trends and the stability of the identified teleconnections. Furthermore, while we have explored the influence of major global climate indices, regional atmospheric circulation patterns and local geographical factors, which can significantly influence precipitation at finer scales, were not examined in detail. The identified correlations between climate indices and precipitation do not establish direct causal relationships; further research employing climate modeling and process-based studies is necessary to elucidate the underlying physical mechanisms driving these connections.

The findings of this study have several important implications. The documented spatial and temporal variability in precipitation underscores the need for region-specific water resource management strategies across Türkiye. Regions with high interannual variability and strong seasonality require more adaptive approaches to water allocation, storage, and drought management. The identified links between large-scale climate indices and regional precipitation patterns offer potential for improved seasonal forecasting, which can inform agricultural planning, disaster preparedness, and water resource management decisions. Considering projected future changes in the phases and intensities of these climate oscillations is crucial for anticipating potential shifts in Türkiye's precipitation regimes under a changing climate, with potential consequences for agriculture, hydropower generation, and ecosystem health. Future research should focus on downscaling these large-scale relationships to regional and local levels, exploring the role of other potential climate drivers, and utilizing climate models to simulate the observed relationships and project future precipitation scenarios for Türkiye. Ultimately, a deeper understanding of these complex precipitation dynamics and their drivers is essential for developing effective climate change adaptation and mitigation strategies in this water-stressed region.

6 Conclusion

This study investigated the relationship between Türkiye's precipitation dynamics and atmospheric-oceanic interactions, revealing significant spatial and temporal variability. While confirming well-known regional contrasts (e.g., high coastal vs. low inland precipitation), the analysis of Precipitation Concentration (PCI), Seasonality Index (SI), and teleconnection indices provides new insights into the mechanisms driving Türkiye's hydroclimatic variability.

Key findings include:

- An evident north-south gradient in precipitation concentration, with coastal regions (particularly the south and west) experiencing higher seasonal variability, while the Black Sea coast maintains more uniform precipitation.
- Decadal shifts in PCI suggest evolving precipitation regimes, possibly linked to large-scale climate modes (AMO, PDO, ENSO).
- Teleconnection analyses reveal that AMO has the strongest coherence with long-term precipitation trends, while PDO and ENSO exhibit more regionally confined and time-sensitive influences.

Seasonal analysis of the Precipitation Concentration Index (PCI) further underscores the diverse precipitation behaviors across Türkiye. The identified high PCI values in the western coastal and southeastern regions during winter, the pronounced concentration in the southern coastal areas during spring, and the extreme concentration in the south and southeast during summer highlight the periods of greatest water availability and potential scarcity in these regions. While previous studies like Yeşilırmak and Atatanır (2016) and Yavuz and Erdoğan (2012) have explored aspects of precipitation variability, our comprehensive seasonal PCI analysis across the entire country provides a more detailed spatial understanding of precipitation concentration dynamics. The consistently low PCI values along the Black Sea coast across all seasons reinforce its distinct hydroclimatic regime.

Importantly, this research extends prior studies by integrating detailed PCI and SI analyses, revealing temporal shifts in precipitation concentration over recent decades and identifying evolving teleconnections with major climate indices such as the AMO and PDO. The findings demonstrate that atmospheric-ocean interactions exert both immediate and lagged influences on precipitation, with regional sensitivity varying across the country. These insights are crucial for anticipating future hydroclimatic changes and underscore the need for region-specific water resource planning and climate adaptation strategies.

This study provides a comprehensive assessment of Türkiye's precipitation dynamics, highlighting significant spatial and temporal variability and elucidating the complex interplay with major climate indices. These findings not only corroborate existing knowledge but also offer a more nuanced understanding of regional precipitation regimes and their sensitivity to large-scale climate oscillations. Future research should focus on further unraveling the drivers behind the observed temporal shifts and exploring the potential impacts of these dynamics on water resources and various sectors across Türkiye.

Acknowledgements The General Directorate of Meteorology (MGM) is to be acknowledged for its contributions to meteorological data.

Author contributions Mehmet Ishak Yuce: Revised manuscript, Musa Esit: Provided data and wrote the manuscript, Ibrahim Halil Deger and Islam YASA: Observed analysis.

Data availability No datasets were generated or analysed during the current study.

Declarations

Conflict of interest The authors declare no competing interests.

References

Abbas S, Kousar S (2021) Spatial analysis of drought severity and magnitude using the standardized precipitation index and streamflow drought index over the upper indus basin, Pakistan. Environ Dev Sustain 23:15314–15340. https://doi.org/10.1007/s10668-021-01299-y

Abdelkader M, Yerdelen C (2022) Hydrological drought variability and its teleconnections with climate indices. J Hydrol 605:127290. https://doi.org/10.1016/j.jhydrol.2021.127290

Ahmadi F, Nazeri Tahroudi M, Mirabbasi R, Kumar R (2022) Spatiotemporal analysis of precipitation and temperature concentration using PCI and TCI: a case study of Khuzestan province, Iran. Theor Appl Climatol 149:743–760. https://doi.org/10.1007/s00704-022-04077-6

Akdi Y, Ünlü KD (2021) Periodicity in precipitation and temperature for monthly data of Turkey. Theor Appl Climatol 143:957–968. https://doi.org/10.1007/s00704-020-03459-y

Aksu HH (2021) Basin-based precipitation potential of Turkey. Arab J Geosci 14:2470. https://doi.org/10.1007/s12517-021-08841-2

Aksu H, Cetin M, Aksoy H et al (2022) Spatial and temporal characterization of standard duration-maximum precipitation over black sea region in Turkey. Nat Hazards 111:2379–2405. https://doi.org/10.1007/s11069-021-05141-6

Alexander LV, Zhang X, Peterson TC et al (2006) Global observed changes in daily climate extremes of temperature and precipitation. J Geophys Res Atmos. https://doi.org/10.1029/2005JD006290

Ali R, Kuriqi A, Abubaker S, Kisi O (2019) Long-term trends and seasonality detection of the observed flow in Yangtze river using Mann-Kendall and sen's innovative trend method. Water 11:1855. https://doi.org/10.3390/w11091855

Ashrafi S, Karbalaee AR, Kamangar M (2024) Projections patterns of precipitation concentration under climate change scenarios. Nat Hazards 120:4775–4788. https://doi.org/10.1007/s11069-024-06403-9

Baltacı H, Akkoyunlu BO, Tayanç M (2018) Relationships between teleconnection patterns and Turkish climatic extremes. Theor Appl Climatol 134:1365–1386. https://doi.org/10.1007/s00704-017-2350-z

Benesty J, Chen J, Huang Y, Cohen I (2009) Pearson correlation coefficient. In: Cohen I, Huang Y, Chen J, Benesty J (eds) Noise reduction in speech processing. Springer, Berlin, pp 1–4

Boughdadi S, Saidi ME, Ait Brahim Y et al (2024) Atlantic and Mediterranean-Sourced precipitation over the maghreb: trends and Spatiotemporal variability. Earth Syst Environ 8:765–782. https://doi.org/10.1007/s41748-024-00426-9

Dai A, Wigley TML (2000) Global patterns of ENSO-induced precipitation. Geophys Res Lett 27:1283–1286. https://doi.org/10.1029/1999GL011140

Dai A, Zhao T, Chen J (2018) Climate change and drought: a precipitation and evaporation perspective. Curr Clim Change Rep 4:301–312. https://doi.org/10.1007/s40641-018-0101-6

Darand M, Pazhoh F (2022) Spatiotemporal changes in precipitation concentration over Iran during 1962–2019. Clim Change 173:25. https://doi.org/10.1007/s10584-022-03421-z

de Luis M, González Hidalgo JC, Raventós J et al (1997) Distribución espacial de la concentración y agresividad de la lluvia en el territorio de la comunidad valenciana. Cuaternario y geomorfología: Rev Soc Española de Geomorfol Asociación Española para el Estudio del Cuaternario 11:33–44

Deniz A, Toros H, Incecik S (2011) Spatial variations of climate indices in Turkey. Int J Climatol 31:394–403. https://doi.org/10.1002/joc.2081

Dong Q, Wang W, Kunkel KE et al (2021) Heterogeneous response of global precipitation concentration to global warming. Int J Climatol 41:E2347–E2359. https://doi.org/10.1002/joc.6851

Dore MHI (2005) Climate change and changes in global precipitation patterns: what do we know? Environ Int 31:1167–1181. https://doi.org/10.1016/j.envint.2005.03.004

Esit M (2022) Investigation of innovative trend approaches (ITA with significance test and IPTA) comparing to the classical trend method of monthly and annual hydrometeorological variables: a case study of Ankara region, Turkey. J Water Clim Change. https://doi.org/10.2166/wcc.2022.356

Esit M, Kumar S, Pandey A et al (2021) Seasonal to multi-year soil moisture drought forecasting. npj Clim Atmos Sci 4:1–8. https://doi.org/10.1038/s41612-021-00172-z

Fischer EM, Knutti R (2015) Anthropogenic contribution to global occurrence of heavy-precipitation and high-temperature extremes. Nat Clim Change 5:560–564. https://doi.org/10.1038/nclimate2617

Gabrielyan H (2024) Historical and geographical overviews of the Euphrates-Tigris and the Orontes basins. In: Gabrielyan H (ed) Turkey's water policy as part of the political strategy: the evolution of Turkey's water policy. Springer Fachmedien, Wiesbaden, pp 107–156

Grinsted A, Moore JC, Jevrejeva S (2004) Application of the cross wavelet transform and wavelet coherence to geophysical time series. Nonlinear Process Geophys 11:561–566. https://doi.org/10.5194/npg-11-561-2004

Gu G, Adler RF (2023) Observed variability and trends in global precipitation during 1979–2020. Clim Dyn 61:131–150. https://doi.org/10.1007/s00382-022-06567-9

Guhathakurta P, Sreejith OP, Menon PA (2011) Impact of climate change on extreme rainfall events and flood risk in India. J Earth Syst Sci 120:359–373. https://doi.org/10.1007/s12040-011-0082-5

Guo E, Wang Y, Jirigala B, Jin E (2020) Spatiotemporal variations of precipitation concentration and their potential links to drought in Mainland China. J Clean Prod 267:122004. https://doi.org/10.1016/j.jclepro.2020.122004

Hao Z, Phillips TJ, Hao F, Wu X (2019) Changes in the dependence between global precipitation and temperature from observations and model simulations. Int J Climatol 39:4895–4906. https://doi.org/10.1002/joc.6111

Held IM, Soden BJ (2006) Robust responses of the hydrological cycle to global warming. https://doi.org/10.1175/JCLI3990.1

Huang J, Ji M, Xie Y et al (2016) Global semi-arid climate change over last 60 years. Clim Dyn 46:1131–1150. https://doi.org/10.1007/s00382-015-2636-8

IPCC (2013) Climate change 2013: the physical science basis. In: TFD Stocker, GK Qin, M Plattner, SK Tignor, J Allen, A Boschung, Y Nauels, V Xia, PM Bex ve, Midgley (eds) Contribution of working group I to the fifth assessment report of the intergovernmental panel on climate change. Cambridge University Press, Cambridge.

Kara Y, Yavuz V, Temiz C, Lupo AR (2024) Exploring spatio-temporal precipitation variations in istanbul: trends and patterns from five stations across two continents. Atmosphere 15:539. https://doi.org/10.3390/atmos15050539

Kendall MG (1975) Rank correlation methods. Griffin, London

Kim J, Porter J, Kearns EJ (2023) Exposure of the US population to extreme precipitation risk has increased due to climate change. Sci Rep 13:21782. https://doi.org/10.1038/s41598-023-48969-7

Kömüşcü AÜ, Aksoy M (2024) Characterizing variability of Spatial patterns of annual and seasonal precipitation of Turkey and identifying the probable driving factors including teleconnection patterns. J Water Clim Change 15:1392–1416. https://doi.org/10.2166/wcc.2024.665

Koycegiz C, Buyukyildiz M (2023) Investigation of Spatiotemporal variability of some precipitation indices in Seyhan basin, turkey: monotonic and sub-trend analysis. Nat Hazards 116:2211–2244. https://doi.org/10.1007/s11069-022-05761-6

Kundzewicz ZW, Kanae S, Seneviratne SI et al (2014) Flood risk and climate change: global and regional perspectives. Hydrol Sci J 59:1–28. https://doi.org/10.1080/02626667.2013.857411

Lehner B, Döll P, Alcamo J et al (2006) Estimating the impact of global change on flood and drought risks in europe: a continental, integrated analysis. Clim Change 75:273–299. https://doi.org/10.1007/s10584-006-6338-4

Liu B, Tan X, Gan TY et al (2020) Global atmospheric moisture transport associated with precipitation extremes: mechanisms and climate change impacts. WIREs Water 7:e1412. https://doi.org/10.1002/wat2.1412

Lu H-L, Li F-F, Gong T-L et al (2023) Reasons behind seasonal and monthly precipitation variability in the Qinghai-Tibet plateau and its surrounding areas during 1979∼2017. J Hydrol 619:129329. https://doi.org/10.1016/j.jhydrol.2023.129329

Mann HB (1945) Nonparametric tests against trend. Econometrica 13:245–259. https://doi.org/10.2307/1907187

Mantua NJ, Hare SR, Zhang Y et al (1997) A Pacific interdecadal climate oscillation with impacts on salmon production

Martin ER, Thorncroft CD (2014) The impact of the AMO on the West African monsoon annual cycle. Q J R Meteorol Soc 140:31–46. https://doi.org/10.1002/qj.2107

Mishra V, Cherkauer KA, Shukla S (2010) Assessment of drought due to historic climate variability and projected future climate change in the Midwestern United States. J Hydrometeorol 11:46–68. https://doi.org/10.1175/2009JHM1156.1

Mrad D, Dairi S, Boukhari S, Djebbar Y (2019) Applied multivariate analysis on annual rainfall in the Northeast of Algeria. J Water Clim Change 11:1165–1176. https://doi.org/10.2166/wcc.2019.272

Mullick MRA, Nur RM, Alam MJ, Islam KMA (2019) Observed trends in temperature and rainfall in Bangladesh using pre-whitening approach. Glob Planet Change 172:104–113. https://doi.org/10.1016/j.gloplacha.2018.10.001

Oliver JE (1980) Monthly precipitation distribution: a comparative index. Prof Geogr 32:300–309. https://doi.org/10.1111/j.0033-0124.1980.00300.x

Qamar S, Ali Z, Sammen SS (2022) A new method for modelling precipitation variability in relation to climate change. J Water Clim Change 14:289–304. https://doi.org/10.2166/wcc.2022.340

Rahmani F, Fattahi MH (2021) A multifractal cross-correlation investigation into sensitivity and dependence of meteorological and hydrological droughts on precipitation and temperature. Nat Hazards 109:2197–2219. https://doi.org/10.1007/s11069-021-04916-1

Ren Y-Y, Ren G-Y, Sun X-B et al (2017) Observed changes in surface air temperature and precipitation in the Hindu Kush Himalayan region over the last 100-plus years. Adv Clim Change Res 8:148–156. https://doi.org/10.1016/j.accre.2017.08.001

Ropelewski CF, Halpert MS (1986) North American precipitation and temperature patterns associated with the El Niño/Southern Oscillation (ENSO)

Rouyer T, Fromentin J-M, Stenseth NC, Cazelles B (2008) Analysing multiple time series and extending significance testing in wavelet analysis. Mar Ecol Prog Ser 359:11–23. https://doi.org/10.3354/meps07330

Safdar F, Khokhar MF, Mahmood F et al (2023) Observed and predicted precipitation variability across Pakistan with special focus on winter and pre-monsoon precipitation. Environ Sci Pollut Res 30:4510–4530. https://doi.org/10.1007/s11356-022-22502-1

Salameh AAM (2024) Using the precipitation concentration index for characterizing the rainfall distribution in the levant. J Water Clim Change 15:1945–1960. https://doi.org/10.2166/wcc.2024.037

Şan M, Nacar S, Kankal M, Bayram A (2024) Spatiotemporal analysis of transition probabilities of wet and dry days under SSPs scenarios in the semi-arid Susurluk basin, Türkiye. Sci Total Environ 912:168641. https://doi.org/10.1016/j.scitotenv.2023.168641

Sariş F, Hannah DM, Eastwood WJ (2010) Spatial variability of precipitation regimes over Turkey. Hydrol Sci J 55:234–249. https://doi.org/10.1080/02626660903546142

Sarkar S, Maity R (2020) Increase in probable maximum precipitation in a changing climate over India. J Hydrol 585:124806. https://doi.org/10.1016/j.jhydrol.2020.124806

Schlesinger ME, Ramankutty N (1994) An oscillation in the global climate system of period 65–70 years. Nature 367:723–726. https://doi.org/10.1038/367723a0

Sen PK (1968) Estimates of the regression coefficient based on Kendall's Tau. J Am Stat Assoc 63:1379–1389. https://doi.org/10.1080/01621459.1968.10480934

Sensoy S, Demircan M, Ulupinar Y (2008) Climate of Turkey. Turkish state meteorological service 401

Sezen C, Partal T (2019) The impacts of Arctic Oscillation and the North sea Caspian pattern on the temperature and precipitation regime in Turkey. Meteorol Atmos Phys 131:1677–1696. https://doi.org/10.1007/s00703-019-00665-w

Tabari H (2020) Climate change impact on flood and extreme precipitation increases with water availability. Sci Rep 10:13768. https://doi.org/10.1038/s41598-020-70816-2

Tao L, Liang XS, Cai L et al (2021) Relative contributions of global warming, AMO and IPO to the land precipitation variabilities since 1930s. Clim Dyn 56:2225–2243. https://doi.org/10.1007/s00382-020-05584-w

Tongal H (2019) Spatiotemporal analysis of precipitation and extreme indices in the Antalya basin, Turkey. Theor Appl Climatol 138:1735–1754. https://doi.org/10.1007/s00704-019-02927-4

Torrence C, Compo GP (1998) A practical guide to wavelet analysis

Torrence C, Webster PJ (1998) The annual cycle of persistence in the El nño/southern Oscillation. Q J R Meteorol Soc 124:1985–2004. https://doi.org/10.1002/qj.49712455010

Turkes M, Turp MT, An N et al (2020) Impacts of climate change on precipitation climatology and variability in Turkey. In: Harmancioglu NB, Altinbilek D (eds) Water resources of Turkey. Springer International Publishing, Cham, pp 467–491

Türkeş M (2003) Spatial and temporal variations in precipitation and aridity index series of Turkey. In: Bolle H-J (ed) Mediterranean climate: variability and trends. Springer, Berlin, pp 181–213

Unal YS, Deniz A, Toros H, Incecik S (2012) Temporal and spatial patterns of precipitation variability for annual, wet, and dry seasons in Turkey. Int J Climatol 32:392–405. https://doi.org/10.1002/joc.2274

Voigt A, Shaw TA (2015) Circulation response to warming shaped by radiative changes of clouds and water vapour. Nat Geosci 8:102–106. https://doi.org/10.1038/ngeo2345

Wai KM, Wang XM, Lin TH et al (2017) Observational evidence of a long-term increase in precipitation due to urbanization effects and its implications for sustainable urban living. Sci Total Environ 599–600:647–654. https://doi.org/10.1016/j.scitotenv.2017.05.014

Walsh RPD, Lawler DM (1981) Rainfall seasonality: description, spatial patterns and change through time. Weather 36:201–208. https://doi.org/10.1002/j.1477-8696.1981.tb05400.x

Wang X, Jiang D, Lang X (2017) Future extreme climate changes linked to global warming intensity. Sci Bull 62:1673–1680. https://doi.org/10.1016/j.scib.2017.11.004

Wu S, Zhao W, Yao J et al (2022) Precipitation variations in the Tai lake basin from 1971 to 2018 based on innovative trend analysis. Ecol Ind 139:108868. https://doi.org/10.1016/j.ecolind.2022.108868

Yang P, Zhang Y, Xia J, Sun S (2020) Investigation of precipitation concentration and trends and their potential drivers in the major river basins of central Asia. Atmos Res 245:105128. https://doi.org/10.1016/j.atmosres.2020.105128

Yavuz H, Erdoğan S (2012) Spatial analysis of monthly and annual precipitation trends in Turkey. Water Resour Manag 26:609–621. https://doi.org/10.1007/s11269-011-9935-6

Yeşilırmak E, Atatanır L (2016) Spatiotemporal variability of precipitation concentration in Western Turkey. Nat Hazards 81:687–704. https://doi.org/10.1007/s11069-015-2102-2

Yetik AK, Arslan B, Şen B (2024) Trends and variability in precipitation across Turkey: a multimethod statistical analysis. Theor Appl Climatol 155:473–488. https://doi.org/10.1007/s00704-023-04645-4

Yu Z, Tang X, Colin C et al (2023) Millennial-scale precipitation variability in the Indo-Pacific region over the last 40 Kyr. Geophys Res Lett. https://doi.org/10.1029/2022GL101646. e2022GL101646

Zhang Q, Li J, Singh VP et al (2013) Influence of ENSO on precipitation in the East river basin, South China. J Geophys Res Atmos 118:2207–2219. https://doi.org/10.1002/jgrd.50279

Zhang X, Hao Z, Singh VP et al (2022) Drought propagation under global warming: characteristics, approaches, processes, and controlling factors. Sci Total Environ 838:156021. https://doi.org/10.1016/j.scitotenv.2022.156021

Zhang W, Zhou T, Wu P (2024) Anthropogenic amplification of precipitation variability over the past century. Science 385:427–432. https://doi.org/10.1126/science.adp0212